applied sciences

MDPI

Article

Design Optimization of Plate-Fin Heat Exchanger in a Gas Turbine and Supercritical Carbon Dioxide Combined Cycle with Thermal Oil Loop

Yue Cao *, Jun Zhan, Jianxin Zhou and Fengqi Si

Key Laboratory of Energy Thermal Conversion and Control of Ministry of Education, School of Energy and Environment, Southeast University, Nanjing 210096, China; zhanjun_2019@seu.edu.cn (J.Z.); zjx@seu.edu.cn (J.Z.); fqsi@seu.edu.cn (F.S.)

* Correspondence: ycao@seu.edu.cn; Tel.: +86-158-2182-1826

Abstract: This paper presents an investigation on the optimum design for a plate-fin heat exchanger (PFHE) of a gas and supercritical carbon dioxide combined cycle which uses thermal oil as intermediate heat-transfer fluid. This may promote the heat transfer from low heat-flux exhaust to a high heat-flux supercritical carbon dioxide stream. The number of fin layers, plate width and geometrical parameters of fins on both sides of PFHE are selected as variables to be optimized by a non-dominated sorting genetic algorithm-II (NSGA-II), which is a multi-objective genetic algorithm. For the confliction of heat transfer area and pressure drop on the exhaust side, which are the objective indexes, the result of NSGA-II is a Pareto frontier. The technique for order of preference by similarity to ideal solution (TOPSIS) approach is applied to choose the optimum solution from the Pareto frontier. Finally, further simulation is performed to analyze the effect of each parameter to objective indexes and confirm the rationality of optimization results.

Keywords: gas turbine; thermal oil loop; supercritical carbon dioxide; plate-fin heat exchanger; optimization

Citation: Cao, Y.; Zhan, J.; Zhou, J.; Si, F. Design Optimization of Plate-Fin Heat Exchanger in a Gas Turbine and Supercritical Carbon Dioxide Combined Cycle with Thermal Oil Loop. *Appl. Sci.* **2022**, *12*, 42. https://doi.org/10.3390/app12010042

Academic Editor: Guan Heng Yeoh

Received: 9 November 2021
Accepted: 14 December 2021
Published: 21 December 2021

1. Introduction

Gas turbines have a strategic position in the field of energy utilization, with the advantages of high-efficiency, flexible operation and a wide range of fuel applications. The development of flexible and high-efficient gas turbine power generation technology is an inevitable demand for creating a low-carbon and high-efficiency energy system [1]. Moreover, it is also important to deal with global climate change and achieve the goal of carbon peak and carbon neutralization [2]. However, medium–high temperature waste heat is often carried by the low-pressure exhaust of gas turbines. The waste heat of gas turbines is of a lower heat flux density compared with solar energy, nuclear energy and other medium–high temperature heat sources, and a higher grade than low-temperature heat sources, which indicates that it is valuable to be recovered. According to the principle of energy cascade utilization, combined power cycles can be used for the recovery and utilization of gas residual heat energy.

In recent years, the research on new types of power cycles using supercritical carbon dioxide (s-CO_2) as working fluid has been studied gradually, and its development prospect in the field of waste heat recovery and gas turbine bottom cycle has been discussed [3]. Compared with steam and organic working mediums, the thermodynamic properties of supercritical carbon dioxide match the gas waste heat parameters better and the design of the devices are more compact and efficient, so that the gas and supercritical CO_2 combined cycle could improve the thermal efficiency of the cycle effectively and realize the efficient utilization of waste heat of gas turbines. Researchers have already focused on the heat exchanger design for heat transfer between supercritical carbon dioxide and other working fluids. Cai et al. [4] proposed a microtube heat exchanger for the heat transfer between

supercritical CO_2 and water. Zendehboudi et al. [5] investigated the heat transfer characteristics of a brazed plate heat exchanger for supercritical CO_2 and water. Du et al. [6] conducted a size optimization study for the heat exchanger which was applied in a marine supercritical CO_2 Brayton cycle. Cai et al. [7] optimized microtube heat exchangers for supercritical CO_2 cooling. Wang and Kissick [8] designed a compact heat exchanger for heat transfer between supercritical CO_2 and liquid sodium. A printed circuit heat exchanger (PCHE) was also suggested for the heat transfer of supercritical carbon dioxide. Although a PCHE had been designed for exhaust gas waste heat recovery [9], the pressure loss in the semi-channels of the PCHE was very large. Moreover, the use of heat transfer medium may promote the heat transfer from low heat-flux exhaust to high heat-flux s-CO_2 stream [10]. In this case, the design of a heat exchanger which shoulders the heat-transfer task seems particularly crucial, and plate-fin heat exchangers (PFHE) are a feasible solution because of their high thermal efficiency and large heat transfer area per unit volume [11]. Among these former heat exchangers, it seems that the plate-fin heat exchanger is a better solution for the gas turbine and supercritical carbon dioxide combined cycle with thermal oil loop.

Several researchers have explored the optimization method for design parameters of plate-fin heat exchangers. Kedam et al. [12] used the heat transfer j correlations to design a compact plate-fin heat exchanger, and results showed that this model was viable for PFHE with offset trip fins and wavy fins. Jige et al. [13] focused on the heat transfer characteristics of vertical upward flow in plate-fin heat exchangers. Guo et al. [14] conducted an optimization for the fin types of multi-stream plate-fin heat exchangers. Haider et al. [15] focused on the inlet configuration design to enhance the thermodynamic performance of plate-fin heat exchangers. Wen et al. [16] carried out a numerical investigation on fin configurations of plate-fin heat exchangers. Moreover, researchers begin to employ artificial intelligence approaches to optimize the design parameters of plate-fin heat exchangers, such as neural networks [17]. Cho et al. [18] used a genetic algorithm to optimize the PFHE layer stacking pattern with low thermal tress in abnormal operating conditions. Zarea et al. [19] employed bees algorithm hybrid with particle swarm optimization to complete a thermal-economic design of plate fin heat exchangers. Li et al. [20] used a multi-objective genetic algorithm to obtain the geometric parameters of serrated fins in PFHE, considering heat transfer enhancement, decrease in flow resistance and maximum stress. NSGA-II is a multi-objective genetic algorithm proposed by Deb et al. [21]. With the advantages of quick speed and good convergence of the solution set, it has been used by a number of researchers [22,23] and has become the benchmark of other multi-objective optimization algorithms [24]. Besides, Hajabdollahi [25] introduced the constructal theory for multi-objective optimization of plate-fin heat exchangers.

In order to make full use of exhaust heat from gas turbines, this paper presents an investigation on the multi-objective optimum design for plate-fin heat exchangers of a gas and supercritical carbon dioxide combined cycle using thermal oil as an intermediate heat-transfer fluid. The heat transfer area and the pressure drop are selected as two optimization objectives, which could show the techno-economic performance of the plate-fin heat exchanger. Firstly, designed thermodynamic parameters for the combined cycle were determined. Based on the geometric estimated model, geometric parameters for the plate-fin heat exchanger in the combined cycle were designed. Moreover, a Non-dominated Sorting Genetic Algorithm-II (NSGA-II) was conducted to find the optimum design result of the plate-fin heat exchanger, considering both the thermo-dynamic performance and compactness. Finally, the objective functions with respect to each parameter are investigated.

2. PFHE Modeling

A counter-flow plate-fin heat exchanger with serrated fins was chosen for the heat transfer of exhaust gas and thermal oil. Its layer structure is shown in Figure 1a, and geometry details of strip-fins are illustrated in Figure 1b.

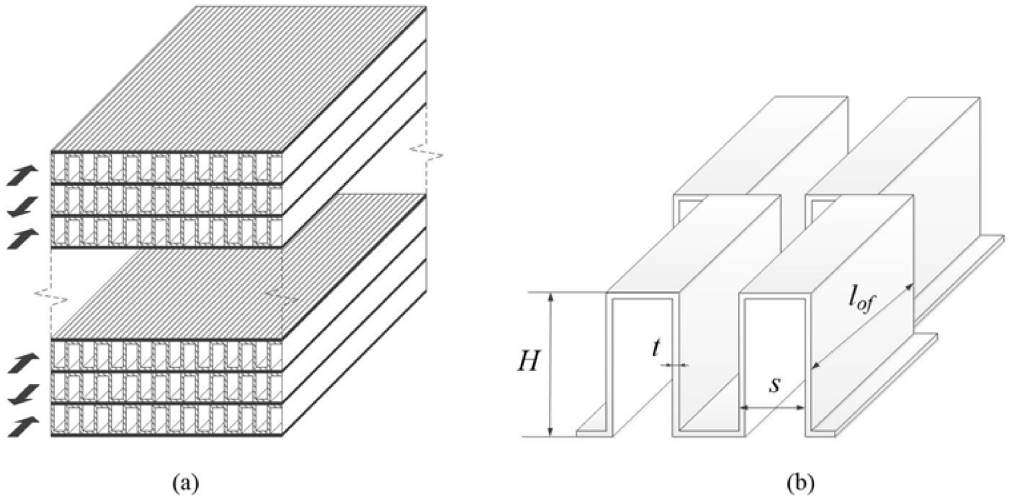

Figure 1. Schematic of PFHE: (**a**) layer structure; (**b**) fins geometry.

2.1. Heat Transfer Calculation

The hot side or cold side of heat transfer area can be calculated by [26]

$$A = LL_W N[1 + 2n(H - t)] \tag{1}$$

The flow area is calculated by the following equation:

$$A_{ff} = (H - t)(1 - nt)L_W N \tag{2}$$

The hydraulic diameter is expressed as

$$D_{hy} = \frac{2(s - t)(H - t)}{[s + (H - t)] + (H - t)t/l_s} \tag{3}$$

For the single-phase region, the j factor is introduced to calculate the heat transfer coefficient for the single-phase flow [11], therefore:

$$h = \frac{jc_p q_m \mathrm{Pr}^{-2/3}}{A_{ff}} \tag{4}$$

As the Joshi and Webb correlation expressed [27,28], the j factor can be given:

$$j = \begin{cases} 0.53Re^{-0.50}(l_s/D_{hy})^{-0.15}[s/(H-t)]^{-0.14} (Re \le Re^*) \\ 0.21Re^{-0.40}(l_s/D_{hy})^{-0.24}(t/D_{hy})^{0.02} (Re \ge Re^* + 1000) \end{cases} \tag{5}$$

$$Re^* = 257(l_s/s)^{1.23}(t/l_s)^{0.58} D_{hy}\left\{t + 1.328\left[Re/\left(l_s D_{hy}\right)\right]^{-0.5}\right\}^{-1} \tag{6}$$

The thermal design of PFHE is carried out by using the ε-NTU method. Counter flow structure is adopted in the present paper, and the relationship between ε and NTU is shown in the following formula:

$$\varepsilon = \frac{1 - \exp\left\{(-NTU)\left[1 - \frac{(q_m c)_{min}}{(q_m c)_{max}}\right]\right\}}{1 - \frac{(q_m c)_{min}}{(q_m c)_{max}} \exp\left\{(-NTU)\left[1 - \frac{(q_m c)_{min}}{(q_m c)_{max}}\right]\right\}} \tag{7}$$

The effectiveness ε, which is defined as the ratio of actual heat transfer to theoretical maximum heat transfer, can be found as:

$$\varepsilon = \frac{(t' - t'')_{max}}{t'_h - t'_c} \tag{8}$$

In this method, the number of transfer units *NTU* is defined as

$$NTU = \frac{1}{(q_m c)\left[\frac{1}{(hA)_h} + \frac{1}{(hA)_c}\right]_{min}} \tag{9}$$

2.2. Pressure Drop Estimation

For laminar or turbulent flow, the friction properties of the PFHE surface can be obtained by the following equations [27]:

$$f = \begin{cases} 8.12Re^{-0.74}(1/D_{hy})^{-0.41}(s/H - t)^{-0.02} & Re \le Re^* \\ 1.12Re^{-0.36}(1/D_{hy})^{-0.65}\left(t/D_{hy}\right)^{0.17} & Re > Re^* \end{cases} \tag{10}$$

Furthermore, the frictional pressure drop for the hot and cold streams can be calculated by:

$$\Delta p = \frac{2f{q_m}^2}{\rho} \times \frac{L}{D_{hy}L^2N^2(H - t)^2(1 - nt)^2} \tag{11}$$

2.3. Thermal Oil Properties

DOWTHERM A heat transfer fluid [29] was selected as the intermediate heat-transfer fluid for its wide operating temperature range from 288 to 673 K. Operating at this upper temperature limit of 673 K enables the highest exergy heat delivery and, finally, the greatest efficiency. Thermal oil properties were evaluated based on manufacturer data, as shown in Figure 2.

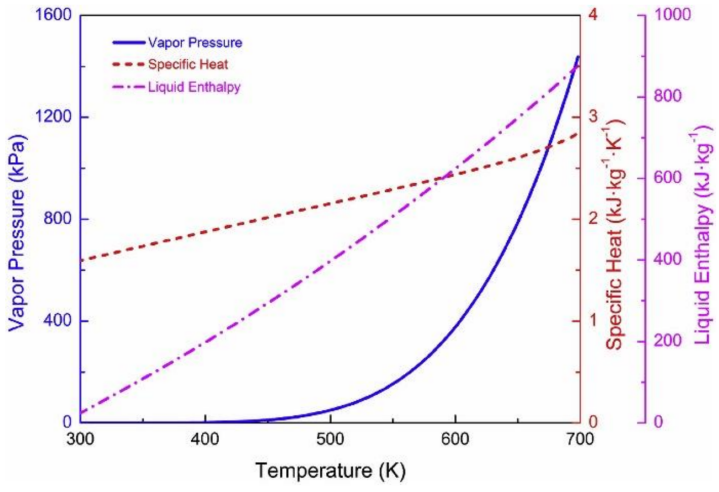

Figure 2. Thermodynamic properties of DOWTHERM A heat transfer fluid.

2.4. Simulation Conditions

Thermodynamic conditions are defined for the plate-fin heat exchanger, including mass flow rate, pressure and temperature in its inlet and outlet, as shown in Table 1. In the following simulations, these conditions are fixed so that comparisons could be conducted for plate-fin heat exchangers with different structure design parameters.

Table 1. Thermodynamic conditions for plate-fin heat exchanger inlet and outlet.

Item	Value
Mass flow rate of exhaust (kg/s)	21.77
Mass flow rate of thermal oil (kg/s)	13.07
Inlet pressure of exhaust (kPa)	105.5
Inlet temperature of exhaust (K)	783
Inlet temperature of thermal oil (K)	397
Outlet temperature of thermal oil (K)	673

Assumptions are made to simplify the thermodynamic conditions in the inlet and outlet of plate-fin heat exchangers, as shown below.

1. The composition of exhaust from gas turbine is fixed;
2. The pressure drop of the exhaust gas in heat exchangers is assumed to be no more than 10% and no less than 3%;
3. The heat exchanger is working steadily and both fluids are assumed to be in the ideal condition.

3. Optimization Method

3.1. Optimization Objectives

In this paper, a multi-objective optimization for the plate-fin heat exchanger is conducted based on its heat transfer area and pressure drop. The heat transfer area represents the capital cost of the plate-fin heat exchanger. The other objective of pressure drop affects the backpressure of the gas turbine and power consumption of the working fluid pump. It indicates that the thermodynamic performance of the combined cycle may change with the variation in pressure drop. In general, the multi-objective optimization is a techno-economic performance optimization for the plate-fin heat exchanger. Therefore, the optimization method proposed in this paper is based on these two optimization objectives.

3.2. Optimization Algorithm

The non-dominated sorting genetic algorithm-II (NSGA-II) is employed to search for the best solutions for the optimization objectives, whose solving procedure is illustrated in Figure 3. The NSGA-II is improved by three approaches compared with NSGA-I. First of all, the use of fast nondominated sorting reduces the complexity of computation and combines the parent population with the offspring population, so that the next generation population is selected from both of the two generations, and the best individuals are all retained. Secondly, elitist preserving ensures that some excellent individuals will not be discarded in the process of evolution, thus the accuracy of the optimization results is improved. Thirdly, crowding distance is employed as the comparison standard among individuals in the population and, as a result, the individuals can be evenly extended to the whole Pareto domain, ensuring the diversity of the population [30]. Moreover, detailed codes for this solving procedure are presented in the Supplementary Materials.

In solving a multi-objective optimization problem, the result is usually not a single global optimum solution which optimizes every objective function simultaneously. Generally, the Pareto frontier is employed to show the distribution of these multi-objective optimization solutions. These solutions can also be called Pareto optimal solutions. To be specific, the Pareto frontier for the plate-fin heat exchanger optimization consists of a horizontal axis of heat transfer area and a vertical axis of pressure drop. Besides, for a given Pareto optimal solution, there is no other solution which satisfies every objective function better than it in variable space, also called the non-dominated solution [31]. In this paper, the NSGA-II is implemented in the platform of MATLAB.

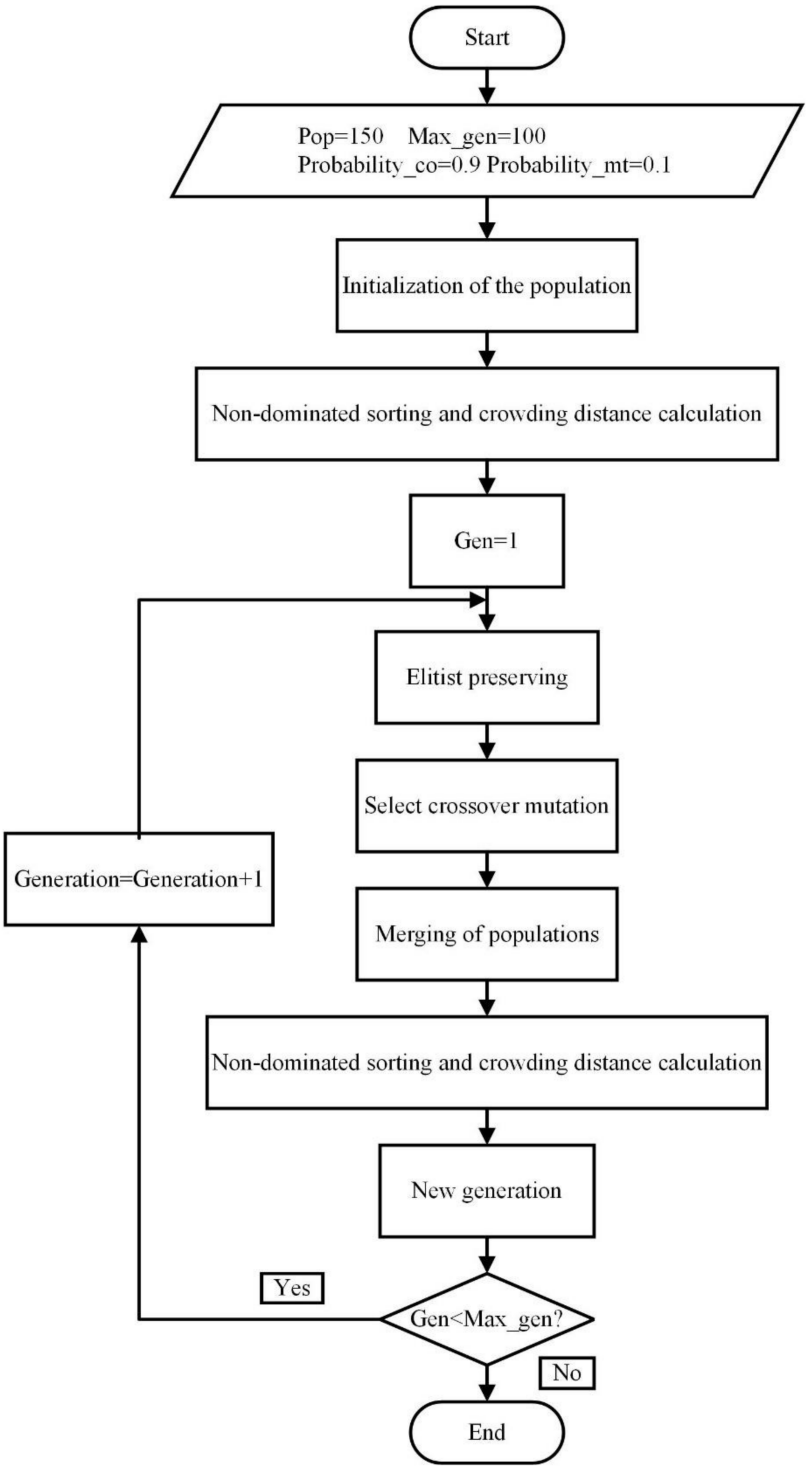

Figure 3. Solving procedure for NSGA-II using plate-fin heat exchanger optimization.

3.3. Decision Variables

As indicators of thermal performance and compactness, the pressure drop on the exhaust side and the heat transfer area of PFHE are selected to be optimization objectives. Ten parameters are chosen as decision variables for the multi-objective optimization of the plate-fin heat exchanger, whose details are listed in Table 2. Moreover, this table also presents specified ranges of these 10 parameters, which are based on reference [26] and the corresponding standards in production practice. With an initial population of 150, the maximum number of generations is 100. Moreover, the crossover probability of 0.9 and a

mutation probability of 0.1 were configurated in the optimization procedure. These control parameters of the NSGA-II have been selected based on some pre-tests done to keep the balance between the computational speed and the convergence property.

Table 2. Decision variables and corresponding specified ranges for multi-objective optimization of plate-fin heat exchanger.

Parameter	Description	Specified Range
N_{hot}	Number of fin layers on hot side	2–200
L_w (m)	Plate width	0.1–5
$l_{s,hot}$ (m)	Offset fin length on hot side	0.03–0.010
$l_{s,cold}$ (m)	Offset fin length on cold side	0.03–0.010
s_{hot} (m)	Spacing of fins on hot side	0.001–0.005
s_{cold} (m)	Spacing of fins on cold side	0.001–0.005
H_{hot} (m)	Height of fins on hot side	0.002–0.020
H_{cold} (m)	Height of fins on cold side	0.002–0.020
t_{hot} (m)	Thickness of fins on hot side	0.0001–0.0005
t_{cold} (m)	Thickness of fins on cold side	0.0001–0.0005

3.4. Optimum Solution Selection

Once the NSGA-II program is completed, one optimum solution should be selected from Pareto frontier as the optimum design for PFHE. Selection criteria can depend on engineering experiences, relative importance of the objective functions, sensitivity of the optimum solutions to the parameters, etc. The technique for order of preference by similarity to ideal solution (TOPSIS) approach is applied in this paper for its wide utilization in choosing appropriate solutions from the Pareto frontier [32]. The principle of the TOPSIS approach is to evaluate every solution by calculating its comprehensive distance between the ideal optimal solution and the ideal worst solution. The solution with the highest score is considered as the optimum decision.

Suppose there are m vectors as the optimization results of n objective functions, as shown in Equation (12).

$$X_i = [X_{i1},\ X_{i2}, \ldots, X_{in}]\ , (i = 1, 2, \ldots, m) \tag{12}$$

Firstly, positive processing is employed on solutions to achieve the largest value of each objective function, as the larger it is, the more favorable it is. As shown in Equation (13), the reciprocals of area and pressure drop were taken in the present paper.

$$\overline{X_{ij}} = \frac{1}{X_{ij}}, (i = 1, 2, \ldots, m), (j = 1, 2, \ldots, n) \tag{13}$$

$$\overline{X_i} = \left[\overline{X_{i1}},\ \overline{X_{i2}}, \ldots, \overline{X_{in}}\right]\ , (i = 1, 2, \ldots, m) \tag{14}$$

Secondly, $\overline{X}_i$ are standardized by

$$Z_{ij} = \frac{\overline{X_{ij}}}{\sqrt{\sum_{k=1}^{m} \left(\overline{X_{kj}}\right)^2}}, (i = 1, 2, \ldots, m), (j = 1, 2, \ldots, n) \tag{15}$$

$$Z_i = [Z_{i1}, Z_{i2}, \ldots Z_{in}], (i = 1, 2, \ldots, m) \tag{16}$$

Then, the ideal optimal solution Z^+ and the ideal worst solution Z^- are defined as the following:

$$Z^+ = \left[Z_1^+, Z_2^+, \ldots Z_n^+\right] = [\max\{Z_{11}, Z_{21}, \ldots, Z_{m1}\}, \max\{Z_{12}, Z_{22}, \ldots, Z_{m2}\}, \ldots, \max\{Z_{1n}, Z_{2n}, \ldots, Z_{mn}\}] \tag{17}$$

$$Z^- = \left[Z_1^-, Z_2^-, \ldots Z_n^-\right] = [\min\{Z_{11}, Z_{21}, \ldots, Z_{m1}\}, \min\{Z_{12}, Z_{22}, \ldots, Z_{m2}\}, \ldots, \min\{Z_{1n}, Z_{2n}, \ldots, Z_{mn}\}] \tag{18}$$

Distance from solution Z_i to Z^+ and Z^- can be calculated by the following equations, in which w_j is defined as the weight of target index j.

$$D_i^+ = \sqrt{\sum_{j=1}^{n} w_j (Z_j^+ - Z_{ij})^2}, (i = 1, 2, \ldots, m) \quad (19)$$

$$D_i^- = \sqrt{\sum_{j=1}^{n} w_j (Z_j^- - Z_{ij})^2}, (i = 1, 2, \ldots, m) \quad (20)$$

Therefore, the score of solution Z_i i.e., X_i is

$$S_i = \frac{D_i^-}{D_i^+ + D_i^-}, (i = 1, 2, \ldots, m) \quad (21)$$

The normalized score of solution Z_i i.e., X_i is calculated by

$$S_{i,norm} = \frac{S_i}{\sum_{k=1}^{m} S_k}, (i = 1, 2, \ldots, m) \quad (22)$$

In the present paper, m is 150, n is 2, w_1 is 0.8 and w_2 is 0.2.

4. Results and Discussion

In this section, critical data and results during the optimization process are given. After obtaining the optimum design of PFHE, sensitivity analysis is employed to investigate the sensitivity of each objective function with respect to that parameter by varying the value of the selected parameter. All calculation processes for the models were implemented in MATLAB. Properties of the exhaust gas were estimated using NIST REFPROP 9.0 [33].

4.1. Preliminary Optimization Results

At the beginning of the optimization, 150 individuals are generated randomly, some of which are show in Table 3 as examples. Pareto optimal frontier is depicted in Figure 4, and every point on the picture is a non-dominated solution. The TOPSIS approach is conducted to evaluate these solutions. Some of the solutions which obtain the highest normalized scores are listed in Table 4 in descending order. Comparing Table 4 with Table 3, it can be noticed that solutions are improved by NSGA-II significantly and distribution is more centralized. The first solution in Table 4, as known from the TOPSIS approach, is the optimum design of PCHE under the conditions of the present paper.

The effect of the design parameters on the heat transfer area and pressure drop of the hot side are analyzed, respectively. While one parameter is analyzed by varying its value, the others remain constant. Sensitivity analysis is conducted to confirm and explain the rationality of the optimization result. In the pictures in this section, blue curves represent the heat transfer area and red curves represent the pressure drop. When the same parameters on two sides are analyzed, solid curves represent the variables of the hot side and dash lines represent the variables of the cold side.

Table 3. Specific individuals in first generation.

N_{hot}	L_w (m)	$l_{s,hot}$ (mm)	$l_{s,cold}$ (mm)	s_{hot} (mm)	s_{cold} (mm)	H_{hot} (mm)	H_{cold} (mm)	t_{hot} (mm)	t_{cold} (mm)	A (m^2)	Δp (kPa)
48.49	1.83	8.75	3.11	1.17	1.68	13.68	15.17	0.36	0.28	782.33	7.77
46.31	1.93	3.61	7.48	1.72	1.18	15.02	8.25	0.36	0.25	831.33	9.13
24.58	4.00	7.32	3.49	1.28	1.54	16.20	3.66	0.20	0.20	936.00	4.49
20.13	4.55	6.57	7.30	2.26	1.31	17.31	4.60	0.25	0.35	938.83	3.64
68.31	1.22	8.76	5.44	1.66	1.11	19.20	14.25	0.44	0.48	779.18	3.08
168.69	0.74	4.32	4.08	1.12	1.04	12.74	12.96	0.47	0.39	649.68	7.14
81.50	2.37	7.95	5.81	1.06	1.30	12.64	10.03	0.47	0.14	975.84	3.84
180.48	0.45	9.71	7.90	1.05	1.02	17.36	10.41	0.43	0.19	651.97	7.53
57.01	1.87	8.46	6.12	1.23	1.19	11.55	15.80	0.35	0.47	771.08	5.66
182.61	0.57	8.96	6.66	1.07	1.52	12.68	14.99	0.11	0.17	957.40	3.91
136.68	1.50	3.22	4.99	1.45	1.29	12.46	2.20	0.44	0.13	922.72	3.96
117.22	0.82	7.41	4.29	1.33	1.86	11.48	14.00	0.28	0.19	893.36	7.84
106.31	1.42	8.37	9.68	1.47	1.10	9.60	3.16	0.15	0.14	855.37	3.33
44.22	3.88	7.41	8.66	1.09	1.05	9.18	5.77	0.34	0.43	712.00	5.28
148.05	0.85	3.60	3.34	1.32	1.85	8.99	7.18	0.16	0.35	839.25	9.75
35.35	3.36	7.94	9.01	2.08	1.09	12.05	5.58	0.47	0.21	969.11	5.71
57.08	1.40	6.52	6.98	1.50	1.20	16.64	5.63	0.39	0.37	681.91	7.10
189.73	0.66	9.39	9.45	1.06	1.13	11.56	15.28	0.38	0.32	828.73	5.57
71.38	0.93	7.53	4.06	1.53	1.42	16.77	3.93	0.24	0.40	706.44	7.85
34.81	1.93	7.65	8.12	1.54	1.99	19.57	14.67	0.27	0.16	989.33	5.47

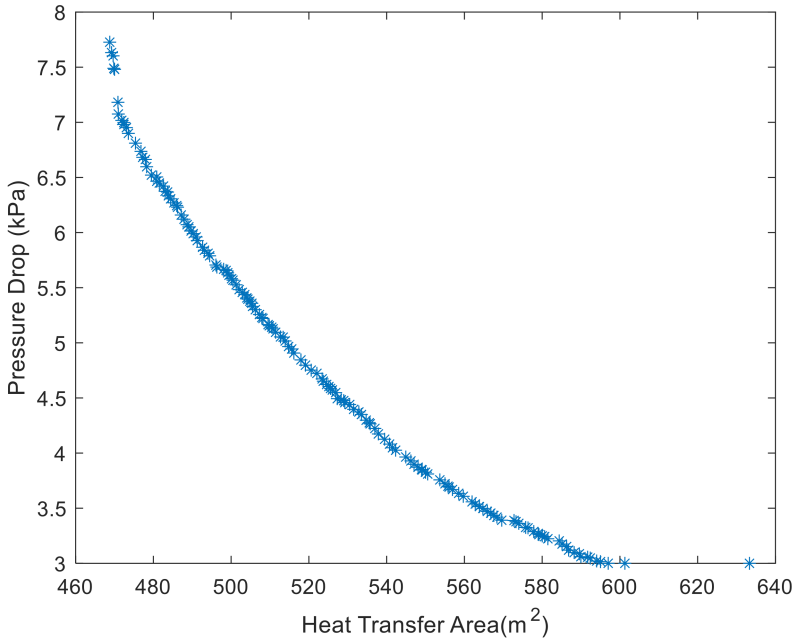

Figure 4. Pareto optimal frontier for heat transfer area and pressure drop of PFHE.

Table 4. Top 20 solutions with highest normalized score.

N_{hot}	L_w (m)	$l_{s,hot}$ (mm)	$l_{s,cold}$ (mm)	s_{hot} (mm)	s_{cold} (mm)	H_{hot} (mm)	H_{cold} (mm)	t_{hot} (mm)	t_{cold} (mm)	A (m^2)	Δp (kPa)	Rank
41.33	1.30	3.74	3.00	1.00	1.00	20.00	13.02	0.10	0.50	526.89	4.55	1
41.47	1.26	9.81	3.00	1.00	1.00	20.00	13.57	0.10	0.50	510.78	5.13	2
41.02	1.16	9.71	3.00	1.00	1.00	20.00	17.02	0.10	0.50	469.65	7.60	3
41.28	1.26	4.47	3.00	1.00	1.00	20.00	14.54	0.10	0.50	504.31	5.40	4
41.08	1.16	5.46	3.00	1.00	1.00	20.00	13.90	0.10	0.50	472.43	6.98	5
41.01	1.21	7.57	3.00	1.00	1.00	20.00	12.37	0.10	0.50	489.71	6.01	6
42.19	1.37	5.34	3.00	1.00	1.00	20.00	14.28	0.10	0.50	580.02	3.25	7
41.33	1.30	10.00	3.00	1.00	1.00	20.00	17.28	0.10	0.50	528.96	4.48	8
42.06	1.27	4.27	3.00	1.00	1.00	20.00	14.69	0.10	0.50	539.48	4.13	9
41.40	1.26	9.97	3.00	1.00	1.00	20.00	13.33	0.10	0.50	514.77	4.97	10
42.18	1.32	4.30	3.00	1.00	1.00	20.00	14.80	0.10	0.50	555.76	3.70	11
40.96	1.21	9.91	3.00	1.00	1.00	20.00	13.62	0.10	0.50	493.13	5.84	12
40.79	1.22	5.69	3.00	1.00	1.00	20.00	14.21	0.10	0.50	488.67	6.07	13
41.04	1.26	10.00	3.00	1.00	1.00	20.00	17.12	0.10	0.50	531.51	4.40	14
42.13	1.29	3.80	3.00	1.00	1.00	20.00	12.94	0.10	0.50	549.13	3.85	15
42.18	1.38	9.70	3.00	1.00	1.00	20.00	17.18	0.10	0.50	569.60	3.39	16
41.36	1.24	8.37	3.00	1.00	1.00	20.00	12.31	0.10	0.50	498.08	5.67	17
41.33	1.25	3.58	3.00	1.00	1.00	20.00	12.90	0.10	0.50	509.82	5.16	18
41.44	1.27	3.89	3.00	1.00	1.00	20.00	14.25	0.10	0.50	520.59	4.75	19
41.04	1.18	3.58	3.00	1.00	1.00	20.00	12.87	0.10	0.50	476.80	6.74	20

4.2. Effect of PFHE Size Parameters

4.2.1. Number of Fin Layers

Above all, it should be noted that there is one more fin layer on the cold side than the hot side. The effect of the number of fin layers on the heat transfer area and pressure drop are illustrated in Figure 5a. In general, the increasing of the number of fin layers causes an increasing in the heat transfer area and a decrease in the pressure drop. The decline in pressure is because of both the decline in Re and the increasing of the number of fin layers. As the number of fin layers increased from 2 to 10, there was a sharp drop in pressure drop; after that, the pressure drop continued down to around 0.1 kPa. There is an obvious change in pressure drop when the number of fin layers is from 10 to 13. From Figure 5b, it can be explained that the increase in the number of fin layers increases the flow area, affecting exhaust changes from turbulence to the laminar flow which makes the j factor increase, and the increase in the heat transfer coefficient on the hot side ultimately results in the reduction of the required heat exchange area. It seems that both heat transfer area and pressure drop are relatively small when the number of fin layers is about 30, which is consistent with the results of the optimization.

4.2.2. Plate Width

First of all, it should be noted that the plate width is designed the same on both sides of PFHE. The effect of the plate width is similar to the number of fin layers. As shown in Figure 6a, when plate width varies from 0 to 0.35, pressure drop drops sharply. As shown in Figure 6b, the changing of pressure drop when the plate width is around 0.5 m has a similar reason as the number of fin layers. It seems that 2.29732 m is reasonable as the width of the plate, taking into account the limit of pressure drop of less than 10%.

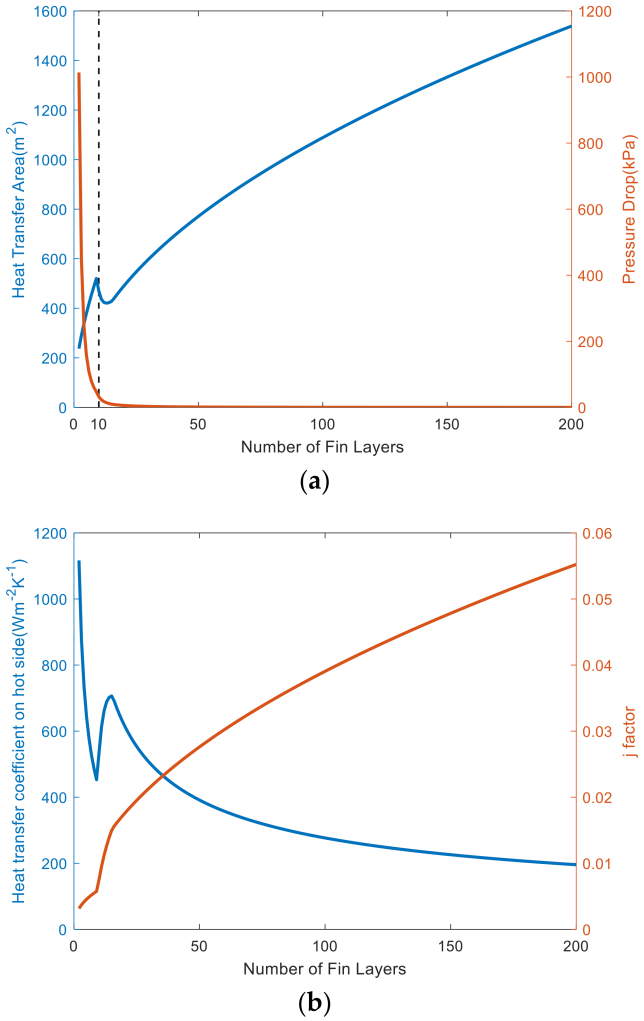

Figure 5. Effect of number of fin layers on heat transfer area and pressure drop of PFHE. (**a**) Heat transfer area, (**b**) heat transfer coefficient on hot side.

4.3. Effect of Fin Design Parameters

4.3.1. Fin Length

As shown in the solid blue and red lines in Figure 7, pressure drop continues to go down, but the heat transfer area continues to increase when fin length on the hot side changes from 3 mm to 10 mm. As for the cold side, both pressure drop and heat transfer area increased persistently when fin length on the cold side changed within the same range. It seems that the optimum design of fin length on the hot side is near 6 mm, which matches the result of the NSGA-II.

4.3.2. Fin Spacing

Figure 8 shows the effect of fin spacing on the heat transfer area and pressure drop. For the fin spacing on the hot side (solid curves in Figure 8), when fin spacing varies from 1 mm to around 3.2 mm, the heat transfer area increases at an accelerating rate and pressure drop descends first then rises to the starting value. When fin spacing varies from around 3.2 mm to around 5 mm, the heat transfer area increases linearly but pressure drop increases slightly. For the fin spacing on the cold side (dash curves in Figure 8), the situation is simpler, both pressure drop and heat transfer area go up in a straight line. Obviously, the spacing of fins on both sides should be near the lower limit, which corresponds to the result of the optimization.

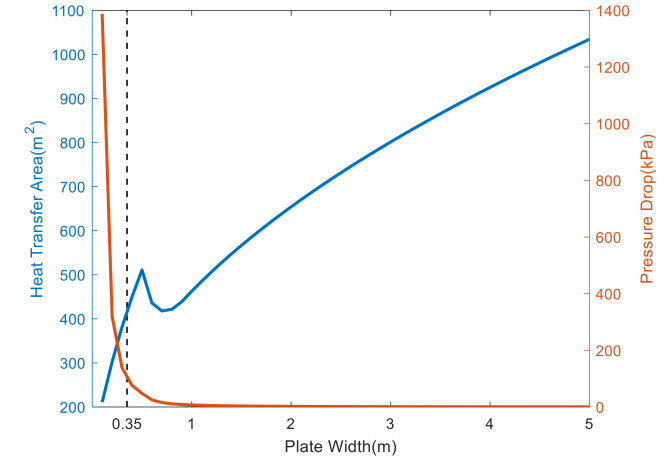

(**a**)

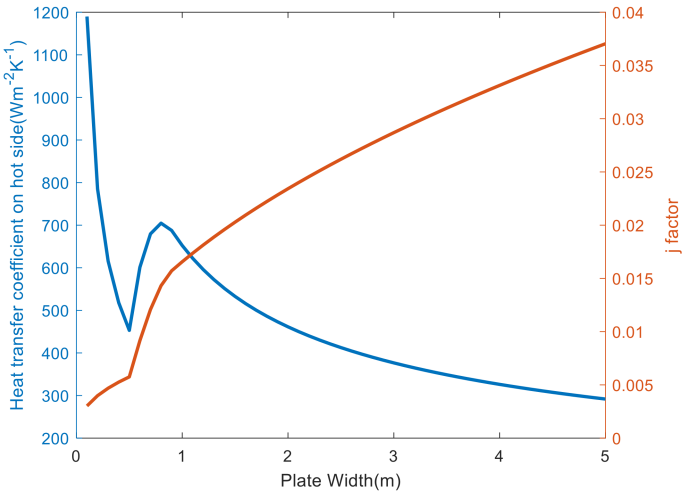

(**b**)

Figure 6. Effect of plate width on heat transfer area and pressure drop of PFHE. (**a**) Heat transfer area, (**b**) heat transfer coefficient on hot side.

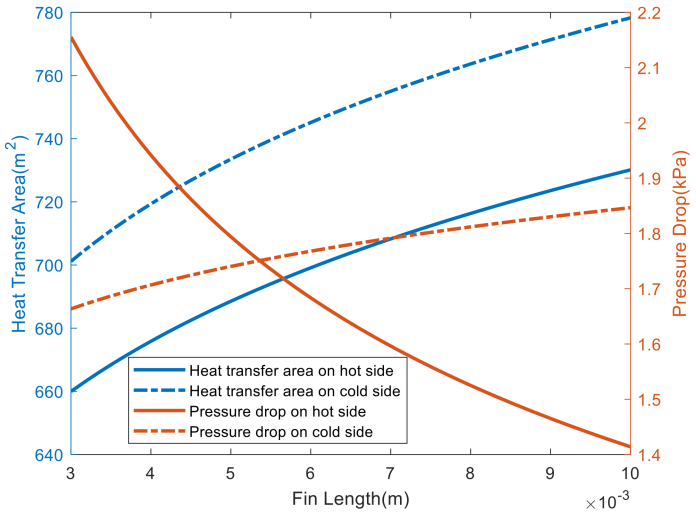

Figure 7. Effect of fin length on heat transfer area and pressure drop of PFHE.

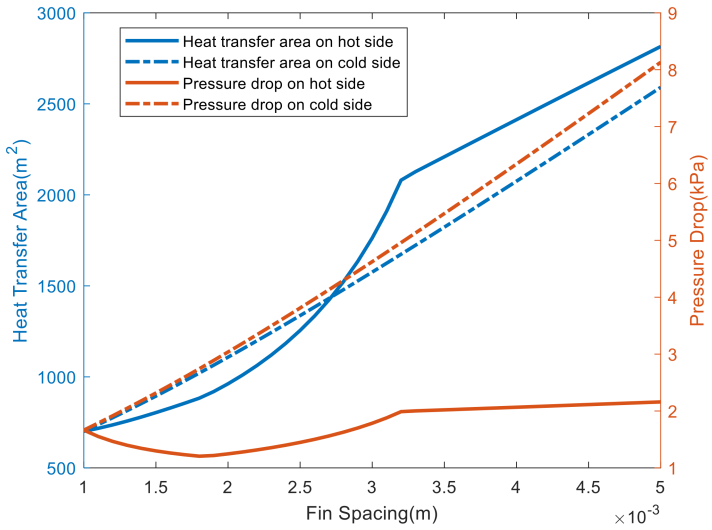

Figure 8. Effect of fin spacing on heat transfer area and pressure drop of PFHE.

4.3.3. Fin Height

The effect of the fin height on both the hot (solid curves) and cold side (dash curves) are illustrated in Figure 9. For fin height on the hot side, as fin height rises, pressure drop descends continuously. Heat transfer area increased linearly when fin height varied from 2 mm to 4 mm, and it experienced a sharp decrease when fin height increased to nearly 8 mm, finally increasing up to when fin height was up to 20 mm. For the fin height on the cold side, it seems fin height has no relation to pressure drop on the hot side, but it does influence heat transfer area. When fin height changed in the same range, the heat transfer area experienced a decelerated decrease stage firstly, finally rising when fin height varied from around 10 mm to 20 mm. According to the above analysis, it seems that 20.00 mm and 13.02 mm are reasonable choices for fin height on the hot and cold side, respectively.

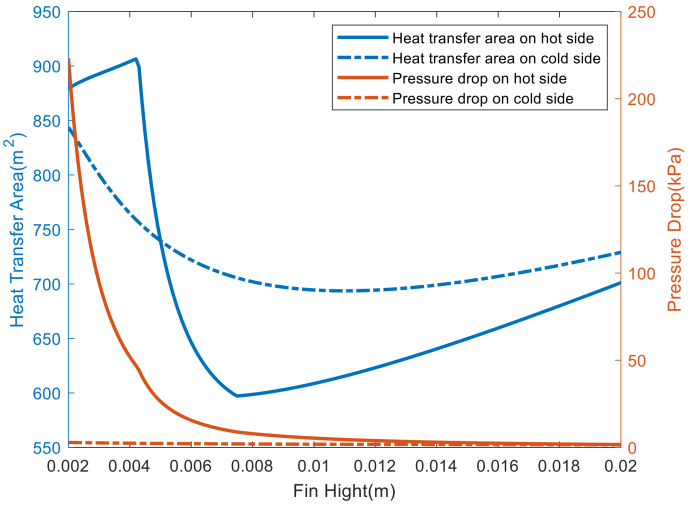

Figure 9. Effect of fin height on heat transfer area and pressure drop of PFHE.

4.3.4. Fin Thickness

The effect of fin thickness on both the hot (solid curves) and cold side (dash curves) are illustrated in Figure 10. For the hot side, the pressure drop increased but heat transfer decreased with fin thickness rising. For the cold side, fin thickness has no influence on pressure drop; however, the increase in fin thickness had a negative impact on heat transfer area. It seems that 0.10 mm and 0.50 mm are reasonable choices for fin thickness on the hot and cold side, respectively.

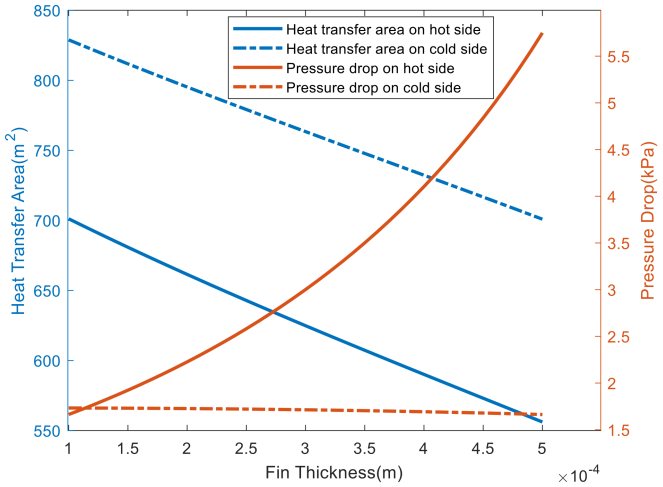

Figure 10. Effect of fin thickness on heat transfer area and pressure drop of PFHE.

5. Conclusions

Parameter optimization was performed for plate-fin heat exchanger of a gas and supercritical carbon dioxide combined cycle using thermal oil as an intermediate heat-transfer fluid, considering heat transfer area and pressure drop as objective indexes, alongside 10 parameters that were used as optimization variables.

The results show that the optimum values of the number of fin layers, plate width, fin length on the hot side and the height of the fins on the cold side are 41.33, 1.30 m, 3.74 mm and 13.02 mm, respectively. Appropriate values of the height of the fins on the hot side and fin thickness on the cold side are near the upper limits, which are 20.00 mm and 0.50 mm, respectively, while suitable values of fin length on the cold side, spacing of fins on the hot side, spacing of fins on the cold side and fin thickness on the hot side are around the lower limits, which are 3.00 mm, 1.00 mm, 1.00 mm and 0.10 mm, respectively. The optimum values of the last five parameters depend on the manufacturing process and standard requirements.

The effect of each parameter on the heat transfer area and pressure drop of plate-fin heat exchanger shows a non-monotonic variation trend. Considering the limitations of pressure drop, a width of the plate of 2.297 m may be reasonable. The simulations with variable fin height show that the reasonable values for the PFHE hot side and cold side are 20.00 mm and 13.02 mm, respectively. Moreover, the suitable design values of fin thickness on the PFHE hot side and cold side are 0.10 mm and 0.50 mm, respectively. These results from this paper indicate that, when optimum design is adopted, PFHE can be used to transfer heat from low heat-flux exhaust to a high heat-flux super-critical carbon dioxide stream with the advantages of compactness and excellent thermodynamic performance. Optimization results and methods used in this paper may help researchers complete the design of PFHEs or carry out further research on optimization.

Supplementary Materials: The following are available online at https://www.mdpi.com/article/10.3390/app12010042/s1, Document S1: Codes for optimization of plate-fin heat exchangers.

Author Contributions: Conceptualization, Y.C. and F.S.; Formal analysis, J.Z. (Jianxin Zhou); Investigation, Y.C. and J.Z. (Jun Zhan); Methodology, Y.C. and J.Z. (Jun Zhan); Software, J.Z. (Jun Zhan) and J.Z. (Jianxin Zhou); Writing—review & editing, Y.C. and F.S. All authors have read and agreed to the published version of the manuscript.

Funding: This research was funded by the Natural Science Foundation of Jiangsu Province (Grant number BK20210240).

Institutional Review Board Statement: Not applicable.

Informed Consent Statement: Not applicable.

Data Availability Statement: The data presented in this study are available on request from the corresponding author.

Conflicts of Interest: The authors declare no conflict of interest.

Nomenclature

A	heat transfer area (m^2)
A_{ff}	flow area (m^2)
c	specific heat (kJ kg^{-1} K^{-1})
c_p	specific heat at constant pressure (kJ kg^{-1} K^{-1})
D_{hy}	hydraulic diameter (m)
f	fanning friction factor
H	fin height (m)
h	heat transfer coefficient (W m^{-2} K^{-1})
j	j factor
L	plate length (m)
L_w	plate width (m)
l_s	offset fin length (m)
N	number of layers
NTU	number of transfer units
n	fin frequency (fins per meter)
p	pressure (Pa)
Δp	pressure drop (Pa)
Pr	Prandtl number
q_m	mass flow rate (kg/s)
Re	Reynolds number
s	fin spacing (m)
t	fin thickness (m)
t'	inlet temperature (K)
t''	outlet temperature (K)
Greek letters	
ε	effectiveness of heat exchanger (%)
ρ	density (kg m^{-3})
Subscripts	
c	cold
h	hot
max	maximum
min	minimum

References

1. Cao, Y.; Dai, Y. Preliminary System Design and Off-Design Analysis for a Gas Turbine and ORC Combined Cycle. *J. Energy Eng.* **2017**, *143*, 04017040. [CrossRef]
2. White, M.T.; Bianchi, G.; Chai, L.; Tassou, S.A.; Sayma, A.I. Review of supercritical CO2 technologies and systems for power generation. *Appl. Therm. Eng.* **2020**, *185*, 116447. [CrossRef]
3. Yu, A.; Su, W.; Lin, X.; Zhou, N. Recent trends of supercritical CO_2 Brayton cycle: Bibliometric analysis and research review. *Nucl. Eng. Technol.* **2020**, *53*, 699–714. [CrossRef]
4. Cai, H.-F.; Jiang, Y.-Y.; Wang, T.; Liang, S.-Q.; Zhu, Y.-M. Experimental investigation on convective heat transfer and pressure drop of supercritical CO2 and water in microtube heat exchangers. *Int. J. Heat Mass Transf.* **2020**, *163*, 120443. [CrossRef]
5. Zendehboudi, A.; Ye, Z.; Hafner, A.; Andresen, T.; Skaugen, G. Heat transfer and pressure drop of supercritical CO2 in brazed plate heat exchangers of the tri-partite gas cooler. *Int. J. Heat Mass Transf.* **2021**, *178*, 121641. [CrossRef]
6. Du, Y.; Hu, C.; Yang, C.; Wang, H.; Dong, W. Size optimization of heat exchanger and thermoeconomic assessment for supercritical CO_2 recompression Brayton cycle applied in marine. *Energy* **2020**, *239*, 122306. [CrossRef]
7. Cai, H.-F.; Jiang, Y.-Y.; Wang, T.; Liang, S.-Q.; Guo, C.; Zhu, Y.-M. An optimization of microtube heat exchangers for supercritical CO2 cooling based on numerical and theoretical analysis. *Int. Commun. Heat Mass Transf.* **2021**, *127*, 105532. [CrossRef]
8. Wang, H.; Kissick, S.M. Modeling and simulation of a supercritical CO2-liquid sodium compact heat exchanger for sodium-cooled fast reactors. *Appl. Therm. Eng.* **2020**, *180*, 115859. [CrossRef]

9. Liu, B.; Lu, M.; Shui, B.; Sun, Y.; Wei, W. Thermal-hydraulic performance analysis of printed circuit heat exchanger precooler in the Brayton cycle for supercritical CO2 waste heat recovery. *Appl. Energy* **2022**, *305*, 117923. [CrossRef]
10. Cao, Y.; Rattner, A.S.; Dai, Y. Thermoeconomic analysis of a gas turbine and cascaded CO2 combined cycle using thermal oil as an intermediate heat-transfer fluid. *Energy* **2018**, *162*, 1253–1268. [CrossRef]
11. Karim, Z.A.; Azmi, M.M.; Abdullah, A. Design of a Heat Exchanger for Gas Turbine Inlet Air using Chilled Water System. *Energy Procedia* **2012**, *14*, 1689–1694. [CrossRef]
12. Kedam, N.; Uglanov, D.; Blagin, E.; Gorshkalev, A. Heat transfer factor j and friction factor f correlations for offset strip fin and wavy fin of compact plate-fin heat-exchangers. *Case Stud. Therm. Eng.* **2021**, *28*, 101552. [CrossRef]
13. Jige, D.; Sugihara, K.; Inoue, N. Evaporation heat transfer and flow characteristics of vertical upward flow in a plate-fin heat exchanger. *Int. J. Refrig.* **2022**, *133*, 165–171. [CrossRef]
14. Guo, K.; Zhang, N.; Smith, R. Design optimisation of multi-stream plate fin heat exchangers with multiple fin types. *Appl. Therm. Eng.* **2018**, *131*, 30–40. [CrossRef]
15. Haider, P.; Freko, P.; Acher, T.; Rehfeldt, S.; Klein, H. Influence of inlet configuration and distributor geometry on the performance of cryogenic plate-fin heat exchangers. *Appl. Therm. Eng.* **2021**, *195*, 117197. [CrossRef]
16. Wen, J.; Li, C.; Hao, H.; Zhao, X.; Lei, G.; Wang, S.; Li, Y. Numerical investigation on fin configuration improvement of 2 K sub-atmospheric plate-fin heat exchangers for the superfluid helium cryogenic systems. *Appl. Therm. Eng.* **2021**, *196*, 117290. [CrossRef]
17. Nascimento, C.; Mariani, V.; Coelho, L. Integrative numerical modeling and thermodynamic optimal design of counter-flow plate-fin heat exchanger applying neural networks. *Int. J. Heat Mass Transf.* **2020**, *159*, 120097.
18. Cho, D.-H.; Seo, S.-K.; Lee, C.-J.; Lim, Y. Optimization of layer patterning on a plate fin heat exchanger considering abnormal operating conditions. *Appl. Therm. Eng.* **2017**, *127*, 1036–1048. [CrossRef]
19. Zarea, H.; Kashkooli, F.M.; Soltani, M.; Rezaeian, M. A novel single and multi-objective optimization approach based on Bees Algorithm Hybrid with Particle Swarm Optimization (BAHPSO): Application to thermal-economic design of plate fin heat exchangers. *Int. J. Therm. Sci.* **2018**, *129*, 552–564. [CrossRef]
20. Li, K.; Wen, J.; Wang, S.; Li, Y. Multi-parameter optimization of serrated fins in plate-fin heat exchanger based on fluid-structure interaction. *Appl. Therm. Eng.* **2020**, *176*, 115357. [CrossRef]
21. Deb, K.; Pratap, A.; Agarwal, S.; Meyarivan, T. A fast and elitist multiobjective genetic algorithm: NSGA-II. *IEEE Trans. Evolut. Comput.* **2020**, *6*, 182–197. [CrossRef]
22. Liu, D.; Huang, Q.; Yang, Y.; Liu, D.; Wei, X. Bi-objective algorithm based on NSGA-II framework to optimize reservoirs operation. *J. Hydrol.* **2020**, *585*, 124830. [CrossRef]
23. Cao, Y.; Dhahad, H.; Mohamed, A.; Anqi, A. Thermo-economic investigation and multi-objective optimization of a novel enhanced heat pump system with zeotropic mixture using NSGA-II. *Appl. Therm. Eng.* **2020**, *194*, 116374. [CrossRef]
24. Shabani-Naeeni, F.; Yaghin, R. Integrating data visibility decision in a multi-objective procurement transport planning under risk: A modified NSGA-II. *Appl. Soft Comput.* **2021**, *107*, 107406. [CrossRef]
25. Hajabdollahi, H. Multi-objective optimization of plate fin heat exchanger using constructal theory. *Int. Commun. Heat Mass Transf.* **2019**, *108*, 104283. [CrossRef]
26. Najafi, H.; Najafi, B.; Hoseinpoori, P. Energy and cost optimization of a plate and fin heat exchanger using genetic algorithm. *Appl. Therm. Eng.* **2011**, *31*, 1839–1847. [CrossRef]
27. Joshi, H.M.; Webb, R.L. Heat transfer and friction in the offset stripfin heat exchanger. *Int. J. Heat Mass Transf.* **1987**, *30*, 69–84. [CrossRef]
28. Ismail, L.S.; Velraj, R.; Ranganayakulu, C. Studies on pumping power in terms of pressure drop and heat transfer characteristics of compact plate-fin heat exchangers—A review. *Renew. Sustain. Energy Rev.* **2010**, *14*, 478–485. [CrossRef]
29. Dowtherm, A. *Heat Transfer Fluid. Product Technical Data*; The Dow Chemical Company: Midland, MI, USA, 1997.
30. Zhang, C.; Wei, H.; Xie, L.; Shen, Y.; Zhang, K. Direct interval forecasting of wind speed using radial basis function neural networks in a multi-objective optimization framework. *Neurocomputing* **2016**, *205*, 53–63. [CrossRef]
31. Cui, Y.; Geng, Z.; Zhu, Q.; Han, Y. Review: Multi-objective optimization methods and application in energy saving. *Energy* **2017**, *125*, 681–704. [CrossRef]
32. Sayyaadi, H.; Mehrabipour, R. Efficiency enhancement of a gas turbine cycle using an optimized tubular recuperative heat exchanger. *Energy* **2012**, *38*, 362–375. [CrossRef]
33. McLinden, M.O.; Klein, S.A.; Lemmon, E.W.; Peskin, A.P. *NSRD12. NIST Thermodynamic and Transport Properties of Refrigerants and Refrigerant Mixtures REFPROP, Version 6.0*; NIST: Gaithersburg, MD, USA, 1998.